

Infrared Microscopic Imaging Analysis

Anselmo Jara, Guillermo Machuca, Sergio Torres and Pablo Gutiérrez

Departamento de Ingeniería Eléctrica, Universidad de Concepción, Casilla 160-C, Concepción, Chile

Keywords: Image Formation, Acquisition Devices and Sensors, Image Enhancement and Restoration.

Abstract: In this paper, we present imaging processing advances and applications of mid-wavelength infrared (MWIR) microscopy imaging. Practical issues related to imaging acquisition, image nonuniformity correction, infrared image quality assessment, and even the MWIR microscope optical Point Spread Function experimental estimation are discussed. The built-up MWIR microscope imaging system allows us to analyse thermal features near to the system diffraction limit, up to 200 frames per second and to focus on less than 2 mm² area. On basis of this technology, our group has been focused efforts in exothermal biological processes, achieving the results exposed in this paper.

1 INTRODUCTION

Infrared (IR) imaging systems enable users to determine the thermal spatial distribution of a target object in a non-invasive manner, and furthermore, without requiring any physical contact between the target and the imaging system. IR imaging sensors are based on the Infrared Focal Plane Array (IRFPA) technology that consists of a mosaic of independent photo-detectors placed at the focal plane of an imaging system (D. A. Scribner et al., 1991).

Every image acquisition system can be considered as a cascade formed set-up, which is mainly composed by a physic interface and an electronic interface. The physic interface is used to focus the irradiance on the IRFPA, even more, in such unit, the image is magnified by an array of lenses. The electronic interface collects the irradiance by means of an IRFPA located exactly in the Focal Plane, to filter and digitalize the electric data as a raw image output data.

Nevertheless, the detectors in the array has unequal responses under a homogeneous stimulus, which leads to the presence of a Fixed Pattern Noise (FPN) noise, well known as Non-uniformity (NU) noise, on the resulting images. Furthermore the lens aberrations effect causes a spatial degradation namely blurring (V. N.Mahajan., 1998). Thus, NU noise and blurring degrade image quality and lead to major difficulties in MWIR microscopic imaging analysis for all kinds of applications.

In the literature, scene-based techniques perform the NU correction (NUC), using only the video sequences that are being imaged, not requiring any kind of laboratory calibration technique (P. M. Narendra., 1980, S. N. Torres and M. M. Hayat, 2003, E. Vera et al., 2011). However in blurring correction, the problem needs to characterize the optical array in order to inversely solve the image degradation. Several deconvolutive methods have been developed to allow the best image restoration (N. Wiener, 1949, W. H. Richardson, 1972, L B. Lucy, 1974).

Our research group is currently working: in MWIR microscopic imaging applications (mainly to exothermal biological processes). Particularly, on MWIR video signal analysis (NUC and de-blurred algorithms and IR imaging performance metrics), and on MWIR microscopic parameters (Diffraction Limit, Instantaneous Field Of View, point spread function (PSF)). Here we present, some of our most recently results.

This paper is structured as follows. In Section 2, we describe the microscopy instrumentation and IR microscopy imaging features are exposed. In Section 3 an experimental PSF estimation method from the IR microscope system is summarized. In Section 4, we tested an algorithm to correct simultaneously the NU noise and blurring artifacts. To evaluate the technique performance, a novel metric is computed in Section 5. Finally, in Section 6 we present the conclusions and future research.

2 IR MICROSCOPY PARAMETERS AND IMAGING SYSTEM FEATURES

2.1 IR Microscopy Parameters

The built-in IR microscope unit is composed of a MWIR camera (Sofradir model EC-IRE 320M) shown in Figure 1, with a HgCdTe FPA transducer that has a spectral response between 3.7 and 4.8 micrometers. The FPA is composed by an array of 320x256 IR detectors, with a 14-bit analog/digital converter with a noise-equivalent temperature difference (NETD) of 10 mK. The FPA can operate up to 320 frames per second. The optical system (IR objective) is integrated by an array of lenses from Janos Technology, allowing a 4X magnification.

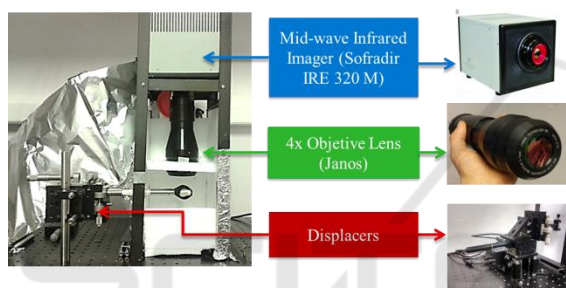


Figure 1: Mid-wave infrared microscope system utilized to acquire microscopic thermal maps.

2.2 System Characterization

The first work was to find the optical system IFoV. For this, images of the USAF Target, were acquired, as shown in Figure 2. The 6th element of 1 group bars was chosen. The length of the bars is known, so that IFoV can be found by dividing the length of said bar by the number of pixels that occupy this object in the image. The second method described in this work is about how to find the diffraction limit. For this purpose, the USAF Target was also used using the Rayleigh criterion (Hecht, 2002) to find the smallest element that can be solved by the Microscope. According to our experiments, such a microscope permits to integrate IR exothermal process with images contained in a 1.99x1.49 mm scene area, with an approximate diffraction limit of 12, 4[μm].

Finally, next performed work corresponds to the determination of a radiometric response curve (temperature). For this, several procedures were employed, giving the best result, the method in which the microscope was located directly in front

of the black body. Video sequences of 10 frames from the black body were taken at different temperatures, from 0 to 100 [$^{\circ}\text{C}$] with intervals of 5 [$^{\circ}\text{C}$] at a controlled ambient temperature of 17 [$^{\circ}\text{C}$]. The results are shown in the Figure 3.

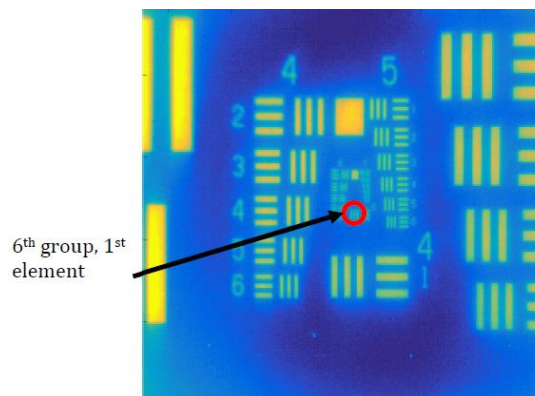


Figure 2: USAF 1951 Target used for the diffraction limit determination. 6th group and 1st element are indicated, last to be solved.

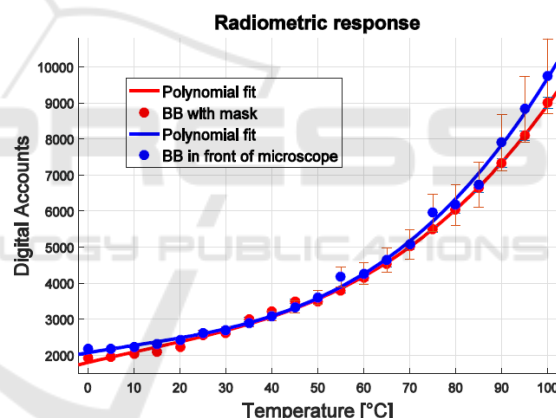


Figure 3: Radiometric response curve using different methods.

3 POINT SPREAD FUNCTION

In this work the applied mathematical foundation for the MWIR microscope PSF estimation, is based on the experimental method proposed in (K. Rossmann., 1969). Where it is assumed that the optical system PSF is isotropic and separable, so it can be computed from the combination of the estimated line PSFs in the x and y axes separately, $h(i)$ and $h(j)$, respectively. Each line PSF can be estimated as the derivative of a sharp transition step function in the desired direction of the scene as follow

$$h(i) = \frac{g'(i)}{B}, \quad h(j) = \frac{g'(j)}{B}, \quad (1)$$

where B is the intensity value of the scene background and $g'(i)$, $g'(j)$ are the step's derivative with respect to x and y direction respectively. These results are obtained by also assuming that the acquisition setup is a linear and shift-invariant system.

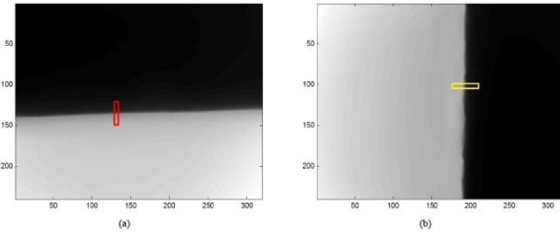


Figure 4: Images of the heat target to produce the desired step functions in the x and y direction.

Finally, and assuming that the PSF varies smoothly in all the other directions, the IR microscope $h(i, j)$ is completed by a 2D Gaussian fit using both components, and enforcing the values of $h(i)$ to $h(j)$.

To produce the needed spatial thermal step, a metal target was cooled down to 5°C and the blackbody radiator source, located at a distance of 20 cm from the microscope optical system, was adjusted to emit at 90 °C. Then, the metal target was positioned at the microscope focal length (2.5 cm) in vertical and horizontal arrangements. Perpendicular linear vectors were extracted from both the x axis (columns) direction and y axis (rows) directions, as depicted in the Figure 4. The estimated PSF can be seen in Figure 5.

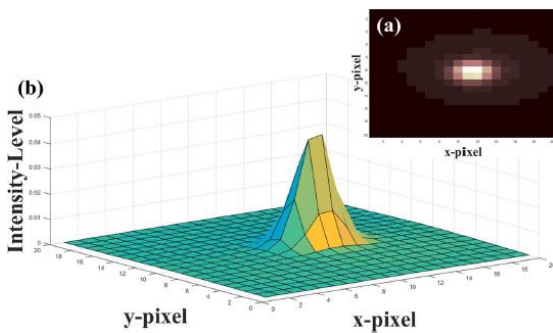


Figure 5: Experimental estimated Point Spread Function, 1.6 standard deviation estimated. a) 2-D image representation. b) 3-D graph representation.

Figure 6 depicts the target images to be used to test the PSF in the de-blurred process. The PSF estimation was applied to a simulated target, for the

blur correction using a blind method and non-blind deconvolution. The blind deconvolution method *Deconvblind* uses an ones-matrix to operate in recursive iterations, estimating a progressive deconvolved image, regardless the use of the infrared microscope PSF.

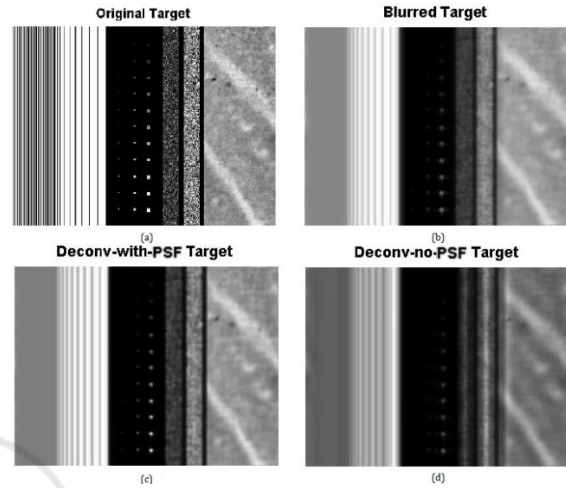


Figure 6: Deconvolution methods no-PSF and using the PSF estimation. (a) Target used for measure the focus level. (b) Blurred target. (c) Target using deconvolution method with use of PSF. And (d) is the target using blind deconvolution method (without uses of PSF).

Figure 7 shows a row-by-row improvement in the RMSE value for the corrected image with the convolution method, using the estimated PSF, in comparison to deconvolution method that do not use the estimated PSF.

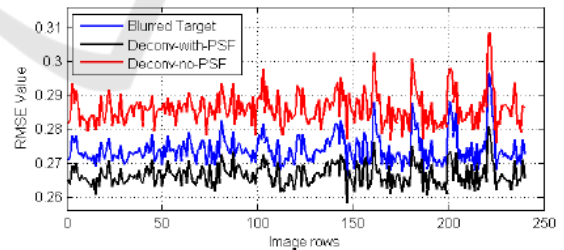


Figure 7: RMSE curves, along the image rows. RMSE for the blurred target (blue), RMSE for the deconvolution with PSF target (black), and RMSE for the deconvolution with PSF target (red).

4 IMAGE DEGRADATION FEATURES ON INFRARED MICROSCOPY

Considering the image acquisition as a cascade

model, where the latent image is degraded, mainly by two stages: The optic stage and the digitalization circuitry. This is, after both steps a MWIR microscopic image suffer a Signal to Noise Ratio (SNR) lower than one, which is mainly produce by two major artefacts blur and NU.

In order to jointly diminish the optical blurring and NU noise on IR microscopic images, we tested here a Joint NU/blur Correction (*JNBC*) method (A. Jara *et al.*).

$$\hat{X}_p(i, j, n) = \frac{\sigma_X[Y(i, j, n) - \mu_Y(i, j, n)]}{\sigma_Y(i, j, n)} + \mu_X \quad (2)$$

Where $\hat{X}_p(i, j, n)$ is a NU-noise-free image, but still degraded by the distortion of the aggregated PSF, $Y(i, j, n)$ is the noisy and blurred imagery, μ_X and σ_X are the global mean and standard deviation, respectively, of the input irradiance, which are known due to the assumption that X follows a Uniform distribution. The quantities $\mu_Y(i, j, n)$ and $\sigma_Y(i, j, n)$ are the mean and standard deviation, respectively, computed with the digital numbers measured from the (i, j) -th detector within the array and using the information available up to the n -th video frame. Normally the mean and standard deviation of the noisy image Y is estimated recursively, which is the approach we adopt here.

$$\hat{X} = \hat{X}_p \left[\frac{\hat{X}_p}{IDFT[DFT[\hat{X}_p] \cdot H(u, v)]} * \hat{h}(i, j) \right] \quad (3)$$

where $H(u, v) = DFT[h(i, j)]$ is the discrete Fourier Transform (DFT) of the estimated PSF and $\hat{h}(i, j)$ is the flipped PSF. As in the numerical implementation of the *Richardson Lucy* algorithm we enforce the denominator in Eq. (3) to have values different from zero. Now, we simply apply inverse filtering over \hat{X} to estimate X , namely

$$X = IDFT \left[\frac{DFT[\hat{X}]}{H(u, v)} \right] \quad (4)$$

In Figure 8 can be appreciated a raw MWIR microscopic image highly corrupted by both NU noise and blur. The *JNBC* method is able to simultaneously compensate for both as shown in Figure 8(b). Significant improvement, in spite of the severity of the NU noise and blur, can be observed with only a naked-eyes evaluation. Moreover, note that as expected, the dead and saturated pixels shown in Figure 8(a) are compensated in the scene by the *JNBC* method.

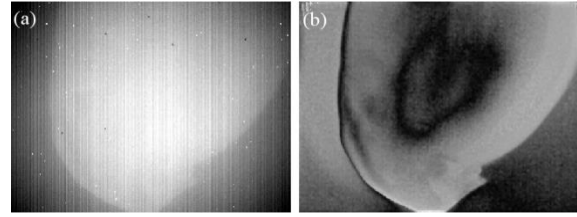


Figure 8: Estimated images using IR Microscopy samples affected by both real NU noise and blur. (a) Raw frame and (b) corrected frame using proposed method. The improved quality of the corrected image can be easily noted at naked eye.

5 INFRARED IMAGE QUALITY ASSESSMENT

We, also here like to test a metric with ability of evaluate jointly blur and NU noise for IR imaging systems. This metric works in the spatial domain applying discrete filtering in order to quantify the edges amount from distinct frequency basis (A. Jara *et al.*).

The *Roughness Laplacian Pattern (RLP)* metric quantifies simultaneously the roughness (NU noise) and the spatial blur on an IR image. It works by combining two measures: the *Laplacian* (∇^2) of the image, in order to quantify the NU noise, and the norm of the discrete *Laplacian of a Gaussian (LoG)* of the image, in order to quantify image edges and details (i.e., measuring the sharpness of the sequence).

$$LP(\hat{X}) = \left[\beta \nabla^2(\hat{X}) + (1 - \beta)[1 - LoG_\sigma(\hat{X})] \right] \quad (5)$$

where β parameter can be used to tune the *RLP* to evaluate IR images with low blurring distortion, e.g., macroscopic IR images (β closer to one), or IR images with high blurring distortion, e.g., microscopic IR images (β closer zero). The *RLP* approaches to zero as the NU noise and/or the image blur is reduced.

The *RLP* metric was evaluated using images with different degradation caused by NU noise and blur, which are shown in the Figures 9 and 11. In Figure 9, each of the simulate images has a fixed level of NU and increases the level of blur, being Figure 9(a) and 9(d) degraded with minor and greater blur, respectively. As can observed in some the structures, e.g. the clock, the edges are not clearly distinguished due to degradation. A different case is perceived in Figure 11, where each simulated images has a fixed level of blur and increases the level of NU noise, this degradation effect can be

better observed when comparing Figure 11 (a) and Figure 11 (d).

Figure 10 shows the results obtained using RLP on the images with fixed NU noise and variable blur. On the left, RLP curves are observed with different sensitivity parameters allowing a change in the value obtained by the metric on the degraded images. In the middle and on the right, the high frequency and low frequency components (NU noise and blur), respectively, are quantified for each image simulated using the terms that compose the proposed metric independently. When we focus on the NU noise, we observe an almost constant trend in the values obtained, which is precisely the effect that we wanted to achieve. On the other hand, the blurring curves increases its values allowing seeing the effect of degradation of blurring on the simulated images.

RLP Curves and independent components of NU noise and blur for different image degradation levels are shown in Figure 12. On the left, we can see that as the sensitivity parameter varies, the RLP obtains other values due to the weight that is granted to each degradation effect. On the other hand, it is seen that the quantized blur effect has very small variations when comparing each value obtained for each case of the degraded images, as shown on the right in Figure 12. This behaviour is totally opposite when we look at the measurement of the NU noise in the center of Figure. Overall, the metric manages to quantify both special effects, separately and mixed, and give a corresponding weight considering the degradation observed.

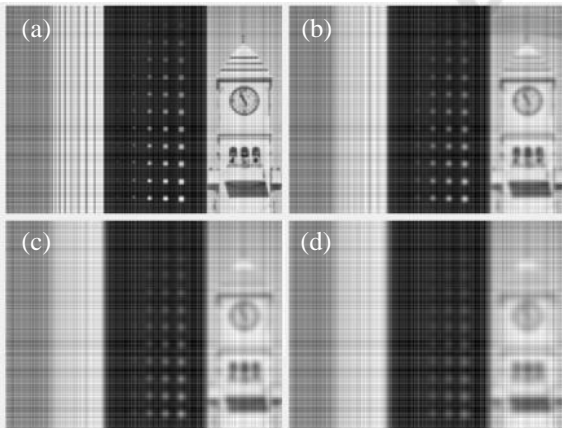


Figure 9: Simulated target image with fixed level of NU (σ^2) and increasing level of Blur (σ). (a) NU $\sigma^2 = 0.3$, $\sigma = 0.23$, (b) NU $\sigma^2 = 0.3$, $\sigma = 0.38$, (c) NU $\sigma^2 = 0.3$, $\sigma = 0.45$, (d) NU $\sigma^2 = 0.3$, $\sigma = 0.47$.

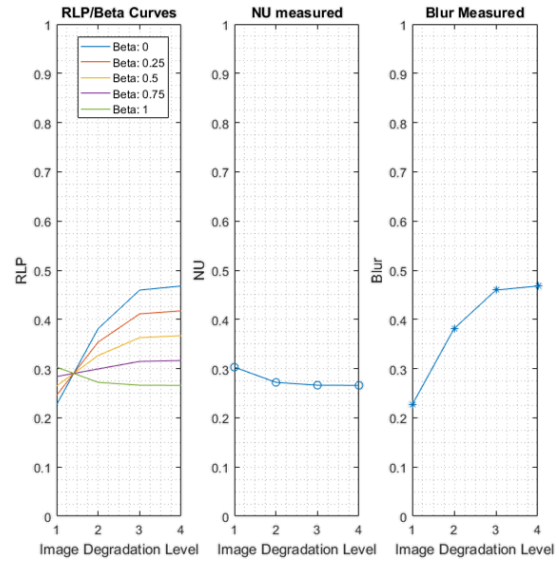


Figure 10: RLP Curves and independent components NU and Blur curves for different image degradation levels. Curves obtained to the simulated target image assessment with fixed level of NU and increasing level of Blur.

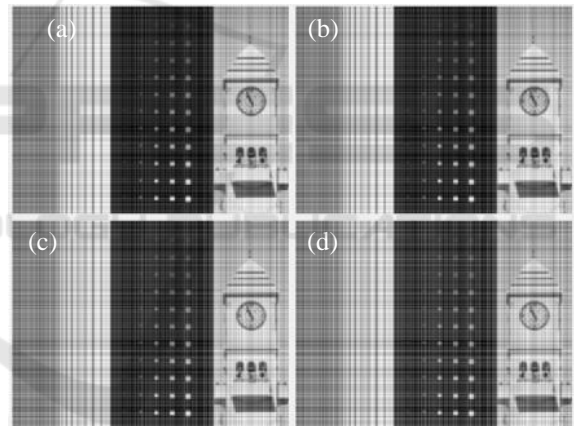


Figure 11: Simulated target image with fixed level of Blur (σ) and increasing level of NU (σ^2). (a) $\sigma = 0.2$, NU $\sigma^2 = 0.3$, (b) $\sigma = 0.2$, NU $\sigma^2 = 0.4$, (c) $\sigma = 0.2$, NU $\sigma^2 = 0.5$, (d) $\sigma = 0.2$, NU $\sigma^2 = 0.6$.

The proposed RLP index is calculated for the in Figure 8 mentioned real IR data sets, showing an improvement from 0.87 to 0.69.

6 CONCLUSIONS

In this paper, advances in mid-wavelength infrared microscopy referred to acquisition, spatial domain infrared image correction, Point Spread Function experimental estimation and image quality

assessment are presented. The key of the PSF estimations is through using deconvolution in a blurred IR-simulated target image showing an improvement when comparison with a blind-deconvolution (no-PSF) method, this is better appreciated in the global RMSE parameter.

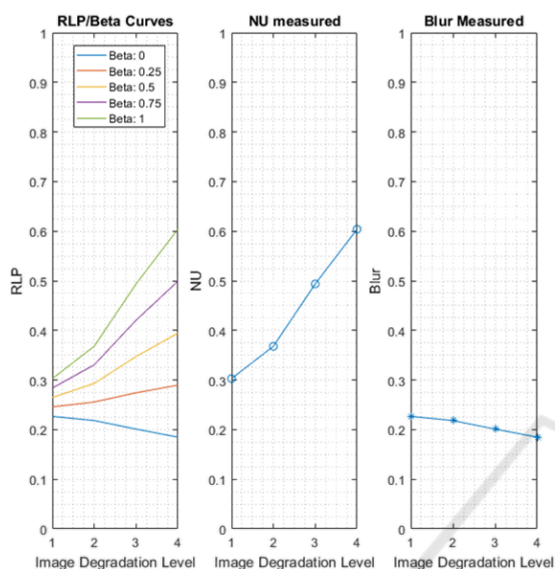


Figure 12: *RLP* Curves and independent components *NU* and *Blur* curves for different image degradation levels. Curves obtained to the simulated target image assessment with fixed level of *Blur* and increasing level of *NU*.

The tested JNBC method combines a well-known NUC algorithm based on constant range statistics and Fourier-based deconvolution method in a single step. Thus, the method has the ability to simultaneously compensating the blurriness and the *NU* noise from degraded IR image sequences, generating an estimation of the true irradiance in scene-based. The assessment of the method has demonstrated that it successfully reduces the *NU/blur*. The performance of the JNBC method is tested in a biological exothermal processes raw datasets with *NU/blur* evidencing an improved image restoration. The proposed *RLP* index is calculated for the mentioned real IR data sets, showing an improvement from 0.87 to 0.69. The improvement on the thermal spatial gradients and resolution of the MWIR microscopic images of the show datasets are quantitatively demonstrated and qualitatively noticeable with naked eyes.

ACKNOWLEDGEMENTS

This research work was partially supported by the

Chilean CONICYT doctoral scholarship program and by FONDECYT grant #1160613.

REFERENCES

- D. A. Scribner, M. R. Kruer, J. M. Killiany,, 1991. Infrared focal plane array technology, Proceedings of the IEEE, 79, 66-85. doi:10.1109/5.64383.
- V. N. Mahajan., 1998. Optical Imaging and Aberrations, Vol. 45.
- P. M. Narendra., 1980. Reference-free nonuniformity compensation for ir imaging arrays. doi:10.1117/12.959478.
- S. N. Torres and M. M. Hayat, 2003. Kalman Filtering for adaptive nonuniformity correction in infrared focal-plane arrays, J. Opt. Soc. Am. A, 20, 470-480.
- E. Vera, P. Meza, and S. Torres, 2011. Total variation approach for adaptive nonuniformity correction in focal-plane arrays, Opt. Lett. 36, (2) ,172-174. doi:10.1364/OL.36.000172.
- N. Wiener, 1949. Extrapolation, interpolation, and smoothing of stationary time series, Vol. 7, MIT press Cambridge, MA.
- W. H. Richardson, 1972. Bayesian-based iterative method of image restoration, 325 JOSA 62 (1), 55-59.
- L. B. Lucy, 1974. An iterative technique for the rectification of observed distributions, The astronomical journal 79, 745.
- Hecht., 2002. Optics. Editorial Addison-Wesley.
- K. Rossmann., 1969. Point spread-function, line spread-function, and modulation transfer function: tools for the study of imaging systems, Radiology 93, (2), 257-272.
- A. Jara, S. Torres, G. Machuca, W. Ramírez, P. A. Gutiérrez, L. A. Viafora, S. E. Godoy, E. Vera, Submitted to Infrared Physics & Technology, Elsevier.
- A. Jara, S. N. Torres, G. Machuca, S. E. Godoy, A non-reference metric for non-uniformity and blurring artifacts on infrared imaging, Unpublished results.